Received: 10 May 2018 | Revised: 10 July 2018 | Accepted: 11 July 2018

DOI: 10.1002/jrs.5460

RESEARCH ARTICLE

WILEY Journal of RAMAN SPECTROSCOPY

Calculation of the optical phonons in ordered Ba_2MgWO_6 perovskite using short-range force field model

J.E. Rodrigues[1,2] | D.M. Bezerra[3] | A.C. Hernandes[1]

[1] Laboratory of Nanomaterials and Advanced Ceramics, São Carlos Institute of Physics, University of São Paulo, São Carlos, Brazil

[2] Optical Spectroscopy and Raman Scattering Research Group, Federal University of São Carlos, São Carlos, Brazil

[3] Department of Chemical Engineering, Federal University of São Carlos, São Carlos, Brazil

Correspondence
J. E. Rodrigues, Laboratory of Nanomaterials and Advanced Ceramics, São Carlos Institute of Physics, University of São Paulo, CEP 13560-970, São Carlos, Brazil.
Email: rodrigues.joaoelias@gmail.com; rodrigues.joaoelias@ifsc.usp.br

Funding information
Conselho Nacional de Desenvolvimento Científico e Tecnológico, Grant/Award Number: 150936/2017-6; Coordenação de Aperfeiçoamento de Pessoal de Nível Superior; Fundação de Amparo à Pesquisa do Estado de São Paulo, Grant/Award Number: 2013/07296-2

Abstract

Ba_2MgWO_6 is a double perovskite tungstate presenting a cubic structure with cubic space group O_h^5. This B-site ordered system has potential applications as microwave ceramics in communication systems. Here, we present our results on the lattice dynamics calculations using short-range force field model to describe both Raman ($\mathbf{A}_{1g} \oplus \mathbf{E}_g \oplus 2\mathbf{F}_{2g}$) and infrared ($4\mathbf{F}_{1u}$) optical phonons at Γ-point of the Brillouin zone in Ba_2MgWO_6 perovskite. Short-range interactions were parameterized through four stretching and three bending force constants in light of the Wilson's GF-matrix method. Satisfactory agreement between experimental and calculated vibrational data was found. We have used the potential energy distribution (PED) coefficients to determine the contribution of each force constant to the optical modes. The PED analysis elucidates that the W atom has a nonnegligible contribution in describing both $\mathbf{A}_{1g}$ breathing and Last-type ($\mathbf{F}_{1u}$) modes. Such a modeling provided insights into vibrational modes, enabling correlation between optical phonons, disorder effects, and physical properties for applications.

KEYWORDS

Ba_2MgWO_6, GF-matrix, group theory, lattice dynamics, ordered perovskite

1 | INTRODUCTION

$A_2B'B''O_6$-type compounds are well-known as talking ceramics for microwave applications, being typically employed as dielectric resonators, antenna, substrates, and filters in high-performance circuitry for satellite and radar systems.[1,2] Improvements in their performance are focusing on the increase of their dielectric constant for miniaturization (ε_r), on the obtention of low dielectric loss for high selectivity ($\tan \delta = Q^{-1}$, where Q is the microwave quality factor), and on a good thermal stability ($\tau_f \sim 0$ ppm.K^{-1}),[3] opening up new frontiers for the Information Communications Technology. In particular, Ba_2MgWO_6 (here after: BMWO) has satisfactory values, including $\varepsilon_r = 15–20$, $Q \times f = 57–82$ THz, and $\tau_f = -38$ ppm.K^{-1}.[4,5] Such a compound can be also used as an appropriated host for Eu^{3+} ions in red emission phosphor.[6] From a crystallographic point of view, BMWO crystal structure arises from the B-site structural ordering process, referred to as 1:1-type, in disordered cubic $Ba(Mg,W)O_3$ perovskite, in which Mg and W atoms are randomly distributed at the same Wyckoff site. In the

ordered state, however, Mg and W populate nonequivalent Wyckoff positions due to their different physical properties, including valences and ionic radii.[7] Such a process has important consequences for applications, mainly in the decrease of dielectric loss of talking ceramics at microwave.[8,9]

Regarding the experimental techniques in identifying the ordering process, Raman and Infrared spectroscopy has advantages over X-ray diffraction, mainly because of its sensibility to detect local disorder and symmetry lowering using optical phonon activity.[8,10] Particularly, the ordered $A_2B'B''O_6$ perovskite with cubic symmetry exhibits four Raman bands in their Raman spectra following the reducible representation $\mathbf{A}_{1g} \oplus \mathbf{E}_g \oplus 2\mathbf{F}_{2g}$. The $\mathbf{A}_{1g}$ breathing-type mode can be applied to evaluate both short- and long-range order achievement in double perovskites by probing its peak parameters such as intensity, position, and width.[11,12] Not only this band but also all the remaining Raman modes can be correlated with the order parameter (η, being extracted from X-ray diffraction data) that describes the degree of long-range order in complex perovskites.[13] In this way, it is desirable to have a detailed description of the atomic motions during each vibrational transition in order to better understand the correlation between optical phonons and disorder in complex perovskites.

While nuclear site group analysis predicts the selection rules for vibrational transition of the phonons at Γ-point ($q \approx 0$), both eigenvalues and eigenvectors are only determined when details on chemical bonds are known and further employed for empirical calculations. In the literature, Liegeois-Duyckaerts and Tarte[14] evaluated the vibrational spectra of $A_2B'B''O_6$ systems, in which A = Sr, Ba, and Pb; B′ = Mg, Ni, Co, Cu, Zn, Cd, Ca, Sr, and Ba; B″ = U, W, Mo, and Te. By using group theory and Cartesian symmetry coordinates, the authors assigned both Raman and infrared modes to the internal modes of oxygen octahedra and translational displacements of A atoms. More recently, Diao et al.[5] determined the optical phonons of BMWO using density functional theory with local density approximation as an *ab initio* method, providing the eigenvector and vibrational pattern of each mode. However, to the best of our knowledge, there are no works reporting force-field study on the optical modes at Γ-point of ordered BMWO perovskites. Such a methodology may elucidate the role of the electronic structure of interatomic bonds into the vibrational spectra.[15,16]

This work aims to describe both Raman and infrared active phonons of ordered cubic Ba_2MgWO_6 perovskite using normal coordinate analysis in context of short-range force field model. Such classical methodology is based on lattice dynamics calculations (LDC) within Wilson's GF-method for solution of the secular equation, representing a rapid and efficient method to assign the vibrational spectra of an arbitrary crystalline structure by generating the complete set of eigenvalues and their respective eigenvectors.[17–19] Indeed, the normal coordinate analysis have been successfully employed to assign the optical modes in several ordered double perovskites, including cubic $Ba_2B'WO_6$[20] and monoclinic $Sr_2B'UO_6$[21] (where B′ = Ni, Co), and monoclinic manganite with chemical formula RE_2CoMnO_6 (where RE = La,[22] Gd[23]). Here, using our results on lattice dynamical study of Ba_2MgWO_6, we briefly discussed possible effects of disorder on the phonon spectra of cubic double perovskites.

2 | CRYSTALLINE STRUCTURE AND GROUP THEORY ANALYSIS

Ordered cubic Ba_2MgWO_6 perovskite belongs to the cubic space group O_h^5 ($Fm\bar{3}m$, No. 225), with lattice constant of 8.10838(6) Å and four formulas per unit cell ($Z = 4$). Such a compound is an example of the 1:1 aristotype highly ordered lattice (or NaCl-type rock-salt), because crystallographic planes containing Mg and W atoms are alternately distributed in the sequence /Mg/W/Mg/W/ along the $[111]_c$ direction of the parental cubic cell.[7] This ordered system also remains stable under high pressure conditions up to 34.3 GPa.[24] Table 1 quotes the atomic positions and Wyckoff sites of Ba, Mg, W, and O atoms, as reported in ICSD Card No. 262318.[7] Based on such data, the selection rules of $q \approx 0$ optical phonons were predicted by using nuclear site group analysis described by Rousseau et al.,[25] as earlier reported in Liegeois-Duyckaerts and Tarte[14]. Here, we have summarized these results for sake of completeness. One can see that Mg and W atoms are centered at different octahedral sites (O_h) and provide only infrared active modes ($\mathbf{F}_{1u}$), as sketched in Figure 1. Indeed, the ordered cubic structure consists of tridimensional network of alternating MgO_6 and WO_6 octahedra, connected at corners. Raman active modes come from Ba and O atoms at 8*c* and 24*e* Wyckoff sites with T_d and C_{4v} local symmetries, following the representation $\mathbf{A}_{1g}$, $\mathbf{E}_g$, and $\mathbf{F}_{2g}$. From this distribution, four Raman ($\mathbf{A}_{1g} \oplus \mathbf{E}_g \oplus 2\mathbf{F}_{2g}$) and four infrared ($4\mathbf{F}_{1u}$) active modes are expected to appear in the vibrational spectra of BMWO compound.

3 | LATTICE DYNAMICS CALCULATIONS

The *VIBRATZ* software package written by Dowty was employed as a framework to solve the secular equation

TABLE 1 Nuclear site group analysis for the ordered Ba_2MgWO_6 cubic lattice

Atom	Site	Symmetry	*x*	*y*	*z*	Phonon contribution at Γ-point
Ba	8*c*	$\bar{4}3m$ (T_d)	0.25	0.25	0.25	$\mathbf{F_{1u}} \oplus \mathbf{F_{2g}}$
Mg	4*a*	$m\bar{3}m$ (O_h)	0	0	0	$\mathbf{F_{1u}}$
W	4*b*	$m\bar{3}m$ (O_h)	0.5	0	0	$\mathbf{F_{1u}}$
O	24*e*	4*m*.*m* (C_{4v})	0.26202(5)	0	0	$\mathbf{A_{1g}} \oplus \mathbf{E_g} \oplus \mathbf{F_{1g}} \oplus \mathbf{F_{2g}} \oplus 2\mathbf{F_{1u}} \oplus \mathbf{F_{2u}}$
$\Gamma_{TOTAL} = \mathbf{A_{1g}} \oplus \mathbf{E_g} \oplus \mathbf{F_{1g}} \oplus 2\mathbf{F_{2g}} \oplus 5\mathbf{F_{1u}} \oplus \mathbf{F_{2u}}$ $\Gamma_{ACOUSTIC} = \mathbf{F_{1u}}$ $\Gamma_{SILENT} = \mathbf{F_{1g}} \oplus \mathbf{F_{2u}}$						
$\Gamma_{RAMAN} = \mathbf{A_{1g}} \oplus \mathbf{E_g} \oplus 2\mathbf{F_{2g}}$ $\Gamma_{INFRARED} = 4\mathbf{F_{1u}}$						

Note. The atomic position and its site symmetry are listed. For more structural details, see ICSD Card No. 262318[7]

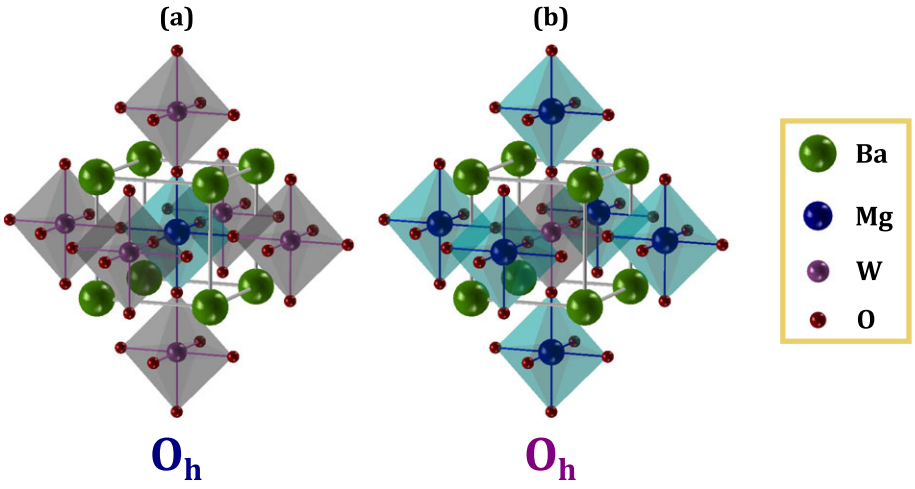

FIGURE 1 (a) MgO_6 and (b) WO_6 octahedra and their O_h site symmetry within the cubic space group O_h^5 ($Fm\bar{3}m$, No. 225). Structural figures were represented with the *ATOMS* software (Version 6.1)[26] [Colour figure can be viewed at wileyonlinelibrary.com]

$|\boldsymbol{F} - \lambda \boldsymbol{G}^{-1}| = 0$ that contains the Wilson's GF-matrix for the LDC.[27] It should be highlighted that the classical theory of the molecular vibration can be found in the seminal work of Wilson, Decius, and Cross.[28] The eigenvalue λ contains the wavenumber ν, since $\lambda = 4\pi^2 c^2 \nu^2$. $\boldsymbol{G}$ has the kinetic energy data, and $\boldsymbol{F}$ denotes the potential energy matrix. Using the internal coordinates represented by $|\boldsymbol{S}\rangle$, both kinetic T and potential V energies can be defined as follows:

$$2T = \langle \dot{\boldsymbol{S}} | \boldsymbol{G}^{-1} | \dot{\boldsymbol{S}} \rangle, \tag{1}$$

$$2V = \langle \boldsymbol{S} | \boldsymbol{F} | \boldsymbol{S} \rangle, \tag{2}$$

where $|\boldsymbol{S}\rangle = \boldsymbol{L}|\boldsymbol{Q}\rangle$. $\boldsymbol{L}$-matrix relates the internal coordinates to normal coordinates, being denoted by $|\boldsymbol{Q}\rangle$ (here, $\boldsymbol{L}^{\dagger} \neq \boldsymbol{L}^{-1}$). For the separable form of the earlier equations, we should have $\boldsymbol{L}^{\dagger}\boldsymbol{G}^{-1}\boldsymbol{L} = \boldsymbol{E}$ (i.e., identity matrix) and, consequently,

$$\boldsymbol{\Lambda} = \boldsymbol{L}^{\dagger}\boldsymbol{F}\boldsymbol{L}, \tag{3}$$

such that $\boldsymbol{\Lambda}$ is a diagonal matrix containing the eigenvalues λ. In particular, the kth component of $\boldsymbol{\Lambda}$ is given by

$$\lambda_k = \sum_{ij} F_{ij} L_{ik} L_{jk} \rightarrow \sum_{ij} \frac{F_{ij} L_{ik} L_{jk}}{\lambda_k} = \sum_{ij} PED_{ij}^{k} = 1. \tag{4}$$

Here, we have defined the potential energy distribution, such that $PED_{ij}^{k} = (F_{ij} L_{ik} L_{jk})/\lambda_k$. Then, the contribution of each force constant toward an arbitrary λ_k can be evaluated through the potential energy distribution (PED) coefficient, that is,

$$PED_{ij}^{k} = \frac{F_{ij} L_{ik} L_{jk}}{\sum_{ij} F_{ij} L_{ik} L_{jk}}, \text{where } F_{ij} = \left(\frac{\partial^2 V}{\partial S_i \partial S_j} \right)_0. \tag{5}$$

In the case of crystals, a total of $(3n-3)$ optical modes are predicted, where n denotes the number of atoms per lattice point within the unit cell. BMWO has 40 atoms in its O_h^5 unit cell and then 10 atoms per lattice point, since a face-centered cubic system has a total of 4 lattice points per unit cell. From these 27 optical vibrations, 9 are Raman active, 12 are infrared active, and 6 are silent,

TABLE 2 Interatomic force constants (i.e., stretching and bending) and their values in units of $N.cm^{-1} \equiv md.\ Å^{-1}$ applied to describe the potential energy matrix

Force constant	Between atoms	Multiplicity	Distance (Å)/angle (°)	Force constant value ($N.cm^{-1}$)
Bonds				
K_1	Ba(8*c*)–O(24*e*)	12	2.868	0.011
K_2	Mg(4*a*)–O(24*e*)	6	2.125	0.404
K_3	W(4*b*)–O(24*e*)	6	1.930	0.722
F_1	O(24*e*)–O(24*e*)	4	2.729	0.415
Angles				
H_1	Ba(8*c*)–O(24*e*)–Mg(4*a*)	4	88.05	0.213
H_2	Ba(8*c*)–O(24*e*)–W(4*b*)	4	91.95	0.640
H_3	O(24*e*)–Ba(8*c*)–O(24*e*)	12	56.81	1.881

as listed in Table 1. The present work is concerned to describe 21 vibrations with Raman ($\mathbf{A}_{1g} \oplus \mathbf{E}_g \oplus 2\mathbf{F}_{2g}$) or infrared ($4\mathbf{F}_{1u}$) activity. Therefore, we have taken as the short-range force constants the stretching (K_i and F_i)- and bending (H_i)-type force constants for the first-neighbor approximation, as summarized in Table 2. The value of each force constant was adjusted by least-square fitting process. The bending forces are included to describe the transverse vibrations in the lattice.[29] The stretching interactions denote the forces between the nearest neighbors Ba–O, Mg–O, W–O, and O–O, while bending forces are described by angles bonds Ba–O–Mg, Ba–O–W, and O–Ba–O. The contribution of each force constant toward an arbitrary calculated mode was estimated using the PED in Equation (5).

4 | RESULTS AND DISCUSSION

In Table 3, we exhibited the Raman and infrared modes calculated from the interatomic force constants of Table 2 along the experimental bands at room temperature extracted from Diao[5] and Liegeois-Duyckaerts and Tarte.[14] The PED coefficient for each calculated optical mode is also shown. As one can verify, there is a satisfactory agreement between those values with a maximum perceptual deviation of ~11%. The optical modes calculated by density functional theory methods reported in Diao et al.[5] are also summarized. Such experimental results are concerned to highly ordered BMWO structure with its order parameter $\eta = 1$, being described by the site distribution listed in Table 1. The complete set of

TABLE 3 List of experimental and calculated Raman ($\mathbf{A}_{1g}$, $\mathbf{E}_g$, and $\mathbf{F}_{2g}$) and infrared ($\mathbf{F}_{1u}$) active modes at room temperature for the ordered Ba_2MgWO_6 perovskite structure

Symmetry	ν Expt. (cm^{-1})[a]	ν Expt. (cm^{-1})[b]	ν DFT. (cm^{-1})[a]	ν LDC. (cm^{-1})[c]	PED coefficient[c] ≥ 10%
Raman modes					
$\mathbf{F}_{2g}(1)$	126	126	105	125	$H_2(25)$, and $H_3(62)$
$\mathbf{F}_{2g}(2)$	441	441	405	432	$F_1(47)$, $H_2(20)$, and $H_3(26)$
$\mathbf{E}_g(1)$	538	-	614	522	$K_2(16)$, $K_3(28)$, $F_1(16)$, $H_2(12)$, and $H_3(24)$
$\mathbf{A}_{1g}(1)$	812	813	833	776	$K_3(13)$, $F_1(29)$, and $H_3(44)$
Infrared modes					
$\mathbf{F}_{1u}(1)$	144	149	111	140	$K_3(24)$, $H_2(26)$, and $H_3(41)$
$\mathbf{F}_{1u}(2)$	284	321	277	256	$K_2(37)$, $K_3(13)$, $H_1(17)$, $H_2(21)$, and $H_3(11)$
$\mathbf{F}_{1u}(3)$	330	381	315	359	$K_2(19)$, $H_1(20)$, $H_2(28)$, and $H_3(17)$
$\mathbf{F}_{1u}(4)$	593	618	619	658	$K_2(11)$, $K_3(16)$, $F_1(28)$, and $H_3(35)$

Note. ν: mode position (in units of cm^{-1}); Expt.: experimental; DFT.: density functional theory; LDC.: lattice dynamics calculations; PED: potential energy distribution.

[a]In Diao et al.[5]

[b]In Liegeois-Duyckaerts and Tarte[14].

[c]In this work.

eigenvectors representing Raman and infrared modes, obtained after solving the secular equation in the description of Wilson, Decius, and Cross[28] is sketched in Figures 2 and 3, respectively. In the next paragraphs, we discuss each optical phonon of the ordered BMWO system.

The $\mathbf{A}_{1g}$ Raman active mode located at 776 cm^{-1} (expt.: 812 cm^{-1}) has major contributions coming from F_1 (stretching bond O–O) and H_3 (angle bond O–Ba–O) force constants, describing breathing-type vibrations of the octahedra: see Figure 2d. Here, Ba atoms are not allowed to move, since their phonon contribution at Γ-point is $\mathbf{F}_{1u} \oplus \mathbf{F}_{2g}$. It should be mentioned that such a mode also depends on the W–O bond (PED ~ 13% for K_3). Such a particular result is in line with experimental data in Liegeois-Duyckaerts and Tarte,[14] in which the $\mathbf{A}_{1g}$ mode position in the Raman spectra of $Ba_2MgB''O_6$ systems (B″ = U, W, Mo, Te) can be associated with the bonding energy E_S of the stretching bond B″–O, that is, $\mathbf{A}_{1g}$(W; 813 cm^{-1}) > $\mathbf{A}_{1g}$(Mo; 779 cm^{-1}) > $\mathbf{A}_{1g}$(U; 753 cm^{-1}) > $\mathbf{A}_{1g}$(Te; 724 cm^{-1}) because E_S(W–O) > E_S(Mo–O) > E_S(U–O) > E_S(Te–O). This fact also

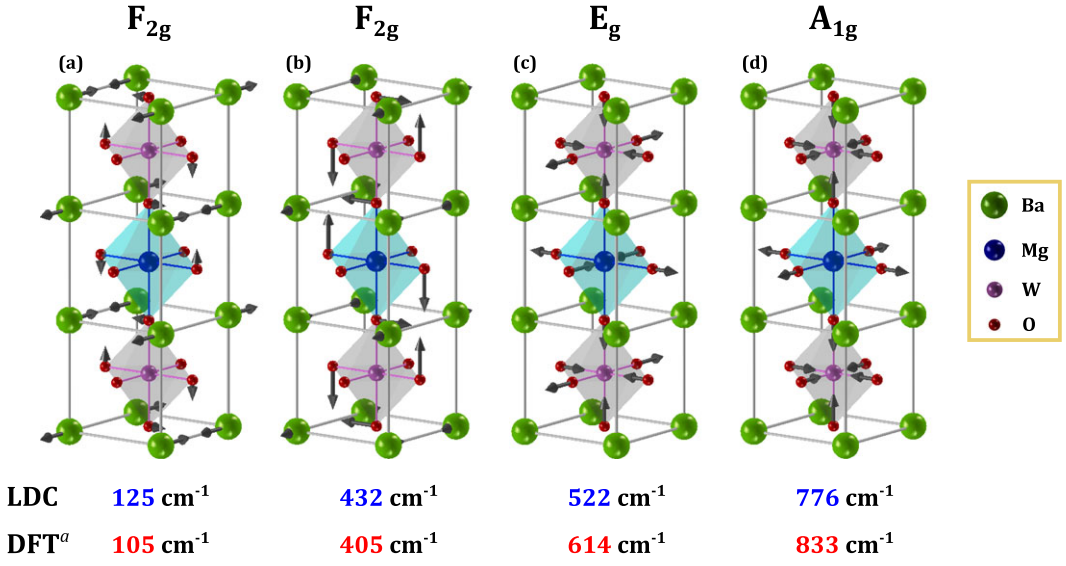

FIGURE 2 Sketches of the Raman active modes ($\mathbf{A}_{1g}$, $\mathbf{E}_g$, and $\mathbf{F}_{2g}$) of the ordered Ba_2MgWO_6 cubic structure, as calculated using short-range force field model. The green, blue, purple, and red spheres denote barium, magnesium, tungsten, and oxygen atoms, respectively. [a] In Diao et al.[5] [Colour figure can be viewed at wileyonlinelibrary.com]

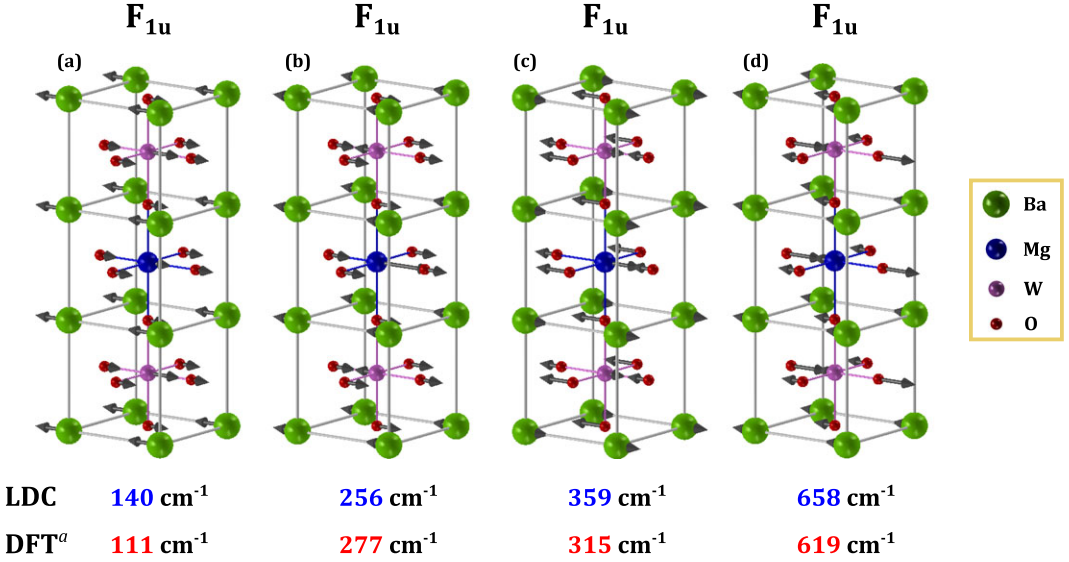

FIGURE 3 Atomic displacements of the infrared active modes ($\mathbf{F}_{1u}$) of the ordered Ba_2MgWO_6 cubic structure, as derived using short-range force field model. The green, blue, purple, and red spheres represent barium, magnesium, tungsten, and oxygen atoms, respectively. [a] In Diao et al.[5] [Colour figure can be viewed at wileyonlinelibrary.com]

corroborates several reported results in the literature concerning the sensibility of $\mathbf{A}_{1g}$ mode to detect B-site local disorder in partially ordered perovskites.[9,30]

In the 1:1 ordered cubic perovskites, the structural disorder usually appears as antisite defects in which 4*a* and 4*b* positions are partially filled by B′ and B″ cations. Unlike the case of the 1:2 ordered perovskites presenting the two-phonon behavior for the $\mathbf{A}_{1g}$ breathing mode,[31,32] antisite process only induces a one-phonon behavior in 1:1 ordered systems. It means that the effect of disorder can be seen by following the peak parameters such as intensity I_0, position ν and width Γ.[9,13] Therefore, partially disordered perovskites only exhibit breathing modes with broadening due to the damping and a downshift attributed to the antisite defects that introduce a variation in the (B′,B″)–O force constant value.

The asymmetric stretching of oxygen octahedra is shown in Figure 2c, denoting the $\mathbf{E}_g$ mode centered at 522 cm^{-1} (expt.: 538 cm^{-1}). Such a mode depends on the stretching bonds Mg–O (PED ~ 16% for K_2) and W–O (PED ~ 28% for K_3), while 24% of PED is due to the angle bond O–Ba–O (H_3). It is noteworthy that such a mode occurs with low intensity in Raman spectra, requiring long spectral acquisition times.[14] Similar to the $\mathbf{A}_{1g}$ mode, Ba atoms are also not allowed to move during this vibration with $\mathbf{E}_g$ symmetry. In Figure 2a, the external mode at 125 cm^{-1} (expt.: 126 cm^{-1}) within $\mathbf{F}_{2g}$ irreducible representation is shown in order to demonstrate the contribution from the motions of Ba atoms. Indeed, the angle bonds Ba–O–W (PED ~ 25% for H_2) and O–Ba–O (PED ~ 62% for H_3) are the most predominant short-range interactions to such a transverse vibration. In this way, the $\mathbf{F}_{2g}$ external mode may show high sensitivity to the lattice modification induced by atomic substitution and strain.[14,33] Another $\mathbf{F}_{2g}$ mode is located at 432 cm^{-1} (expt.: 441 cm^{-1}) with contributions arising from repulsive force between O–O (PED ~ 47% for F_1) and bending force constants for angles Ba–O–W (PED ~ 20% for H_2) and O–Ba–O (PED ~ 26% for H_3). As sketched in Figure 2b, this mode denotes a twist vibration of oxygen octahedra combined with small displacements of Ba atoms.

The infrared active modes of the aristotype perovskites receive special designation, namely, Last, Slater, or Axe, depending on their wavenumber region.[34] Last-type vibrational mode located at 140 cm^{-1} (expt.: 144 cm^{-1}) is drawn in Figure 3a, in which angle bond O–Ba–O (bending force constant H_3) has 41% of contribution to PED. As one can note, Ba atom lattice and oxygen octahedra move in opposite directions, contributing to the unit cell dipole moment and, consequently, affecting the static dielectric constant of the system. The W atom also plays a role in this infrared active mode, since the force constants K_3 (bond W–O) e H_2 (angle Ba–O–W) have contributions to PED of 24% and 26%, respectively. Indeed, reported investigations on the infrared reflectivity spectra of double perovskites have demonstrated that Last-type modes have the greatest dielectric strength and then play a pivotal role in the static dielectric constant at infrared frequencies.[22,35] The $\mathbf{F}_{1u}$ mode located at 658 cm^{-1} (expt.: 593 cm^{-1}) depends mainly on the repulsive force between O–O (PED ~ 28% for F_1) and bending force for angle bond O–Ba–O (PED ~ 35% for H_3). In this Axe-type mode, equatorial oxygen, Ba, Mg, and W atoms move against the apical oxygens, as seen in Figure 3d.

Slater-type vibrational modes centered at 256 and 359 cm^{-1} (expt.: 284 and 339 cm^{-1}) are attributed to the out-of-phase unidirectional displacement of Mg and W ions relative to oxygen anions, as shown in Figures 3b,c. This kind of movement, that is, (Mg, and W)–O beating, tends to induce ferroelectric instabilities in perovskite-like crystal structure, such as $BaTiO_3$ and $KNbO_3$, since the B-site cation moves against the oxygen octahedra cage. It should be mentioned that stretching bond between Mg–O (force constant K_2) are more predominant than that between W–O (force constant K_3). For the $\mathbf{F}_{1u}$ mode drawn Figure 3c, one can clearly observe an antisymmetric bending-type mode of oxygen octahedra combined with slight displacements of Ba atoms.

Unlike the aristotype ABO_3 perovskite belonging to the cubic space group O_h^1 ($Pm\bar{3}m$, No. 221) with only infrared active optical modes, the B-site ordered perovskite $A_2B'B''O_6$ in its aristotype form with cubic space group O_h^5 has optical modes with both Raman and infrared activities.[36,37] As shown above, these modes are seen as a combination of lattice modes (or external motions) and free vibrations of an octahedron (or internal motions).[14,38] From Figures 2 and 3, it is easy to identify the atomic displacement patterns denoting optical modes of an octahedral XY_6-type molecule. Based on group theory calculations, the vibrational spectra of XY_6 free octahedral unit should contain three Raman and two infrared active modes: $\nu_1(\mathbf{A}_{1g}) \oplus \nu_2(\mathbf{E}_g) \oplus \nu_3(\mathbf{F}_{1u}) \oplus \nu_4(\mathbf{F}_{1u}) \oplus \nu_5(\mathbf{F}_{2g})$. A sixth mode $\nu_6(\mathbf{F}_{2u})$ is both Raman and infrared inactive.[39] Regarding those modes with Raman activity, ν_1, ν_2, and ν_5 present totally symmetric stretching, antisymmetric stretching, and symmetric bending of the free octahedron, respectively. This fact enables fundamental investigations on the basic properties of oxygen octahedron, since its Wyckoff site within cubic lattice has O_h point symmetry.

Raman and infrared spectroscopy became a useful tool to probe local disorder at B-site and octahedral tilting in ordered perovskites by analyzing peak parameters such as intensity, position, width, and possible

asymmetry.[8,9,40,41] As a result of disorder, the $\mathbf{A}_{1g}$ mode starts to depict a broadening as a consequence of the antisite defects. From Figure 2d, it is not difficult to realize that a partial occupation of 4*b* sites by Mg and W may introduce a damping of the vibration owing to differences between the stretching force constant K_2 (Mg–O) and K_3 (W–O). In this way, the increase in damping leads to a decreased phonon lifetime and then an enlarged width.[42,43] Confinement effects induced by ordered domains at nanoscale are also reported. Here, contributions coming from phonons located outside the Brillouin zone center may induce peak asymmetry and broadening.[44] Although some papers have investigated the particle size effects for evaluating the phonon confinement in binary oxides, including TiO_2[45] and CeO_2,[46] a detailed study concerning the role of ordered domains and their microstructure on both Raman and infrared spectra of partially ordered perovskites remains scarce.

5 | CONCLUSION

In summary, we have successfully applied the short-range force field model to assign the Raman and infrared modes at Γ-point of ordered Ba_2MgWO_6 perovskite at room temperature. In this calculation, four stretching and three bending force constants were taken to parameterize the nearest neighbor interactions. The calculated optical modes are in reasonable agreement with available experimental results reported in literature. The contribution of each force constant to the optical modes has been derived in light of the PED coefficient. We have shown that $\mathbf{A}_{1g}$ Raman band has contributions coming from stretching bonds O–O and W–O, describing a ν_1-like mode of the XY_6 molecule. The infrared active lattice mode at 140 cm^{-1} (expt.: 144 cm^{-1}) is mainly described by the angle bond O–Ba–O, but there is also a dependence on W atom through stretching and angle bonds W–O and Ba–O–W. Based on our classical calculations, we have analyzed the main effects of the antisite defects on the Raman spectra of cubic $A_2B'B''O_6$ perovskites.

ACKNOWLEDGEMENTS

The authors are grateful to the Brazilian funding agencies: CAPES, CNPq (Grant/Award Number: 150936/2017-6), and FAPESP (Grant/Award Number: 2013/07296-2). We thank the anonymous reviewers for their constructive comments.

ORCID

J.E. Rodrigues http://orcid.org/0000-0002-9220-5809

REFERENCES

[1] M. T. Sebastian, R. Ubic, H. Jantunen, *Int. Mater. Rev.* **2015**, *60*, 392.

[2] I. M. Reaney, D. Iddles, *J. Am. Ceram. Soc.* **2006**, *89*, 2063.

[3] M. Sebastian, *Dielectric Materials for Wireless Communication, Elsevier*, 1st ed. **2008**.

[4] D. D. Khalyavin, J. Han, A. M. R. Senos, P. Q. Mantas, *J. Mater. Res.* **2003**, *18*, 2600.

[5] C.-L. Diao, C.-H. Wang, N.-N. Luo, Z.-M. Qi, T. Shao, Y.-Y. Wang, J. Lu, F. Shi, X.-P. Jing, *J. Am. Ceram. Soc.* **2013**, *96*, 2898.

[6] B. Han, B. Liu, J. Zhang, H. Shi, *Opt. - Int. J. Light Electron Opt.* **2017**, *131*, 764.

[7] B. E. Day, N. D. Bley, H. R. Jones, R. M. McCullough, H. W. Eng, S. H. Porter, P. M. Woodward, P. W. Barnes, *J. Solid State Chem.* **2012**, *185*, 107.

[8] A. Dias, R. L. Moreira, *J. Appl. Phys.* **2003**, *94*, 3414.

[9] R. X. Silva, A. S. de Menezes, R. M. Almeida, R. L. Moreira, R. Paniago, X. Marti, H. Reichlova, M. Maryško, M. V. dos S. Rezende, C. W. A. Paschoal, *J. Alloys Compd.* **2016**, *661*, 541.

[10] A. Ayala, C. Paschoal, I. Guedes, W. Paraguassu, P. Freire, J. Mendes Filho, R. Moreira, J.-Y. Gesland, *Phys. Rev. B* **2002**, *66*, 214105.

[11] R. L. Moreira, F. M. Matinaga, A. Dias, *Appl. Phys. Lett.* **2001**, *78*, 428.

[12] P.-J. Chang, C.-T. Chia, I.-N. Lin, J.-F. Lee, C. M. Lin, K. T. Wu, *Appl. Phys. Lett.* **2006**, *88*, 242907.

[13] I. Levin, S. A. Prosandeev, J. E. Maslar, *Appl. Phys. Lett.* **2005**, *86*, 11919.

[14] M. Liegeois-Duyckaerts, P. Tarte, *Spectrochim. Acta Part a Mol. Spectrosc.* **1974**, *30*, 1771.

[15] S. Brown, H. C. Gupta, J. A. Alonso, M. J. Martínez-Lope, *Phys. Rev. B* **2004**, *69*, 54434.

[16] L. Martín-Carrón, A. De Andrés, M. J. Martínez-Lope, M. T. Casais, J. A. Alonso, *Phys. Rev. B - Condens. Matter Mater. Phys.* **2002**, *66*, 1.

[17] E. Dowty, *Phys. Chem. Miner.* **1987**, *14*, 122.

[18] Y. M. Jana, S. Nandi, H. C. Gupta, *J. Mol. Struct.* **2018**, *1154*, 463.

[19] S. P. Marcondes, J. E. F. S. Rodrigues, M. R. B. Andreeta, A. C. Hernandes, *Vib. Spectrosc.* **2014**, *73*, 144.

[20] S. Garg, M. M. Sinha, H. C. Gupta, *Phys. B* **2014**, *433*, 107.

[21] H. C. Gupta, P. Ashdhir, *Phys. B* **2011**, *406*, 2811.

[22] R. X. Silva, R. L. Moreira, R. M. Almeida, R. Paniago, C. W. A. Paschoal, *J. Appl. Phys.* **2015**, *117*, 214105.

[23] R. X. Silva, H. Reichlova, X. Marti, D. A. B. Barbosa, M. W. Lufaso, B. S. Araujo, A. P. Ayala, C. W. A. Paschoal, *J. Appl. Phys.* **2013**, *114*, 194102.

[24] S. Meenakshi, V. Vijayakumar, S. N. Achary, A. K. Tyagi, *J. Phys. Chem. Solids* **2011**, *72*, 609.

[25] D. L. Rousseau, R. P. Bauman, S. P. S. Porto, *J. Raman Spectrosc.* **1981**, *10*, 253.

[26] E. Dowty, *Software ATOMS 6.1*, Shape Software **2006**.

[27] E. Dowty, *Phys. Chem. Miner.* **1987**, *14*, 67.

[28] E. B. Wilson, J. C. Decius, P. C. Cross, *Molecular Vibrations: The Theory of Infrared and Raman Vibrational Spectra*, Dover Publications **1955**.

[29] L. S. Kothari, A. K. Ghatak, S. Bala, *Am. J. Phys.* **1971**, *39*, 166.

[30] F. Jiang, S. Kojima, C. Zhao, C. Feng, *J. Appl. Phys.* **2000**, *88*, 3608.

[31] J. E. F. S. Rodrigues, P. J. Castro, P. S. Pizani, W. R. Correr, A. C. Hernandes, *Ceram. Int.* **2016**, *42*, 18087.

[32] S. R. Kiran, G. S. Babu, C. Narayana, V. R. K. Murthy, V. Subramanian, *Mater. Res. Bull.* **2013**, *48*, 194.

[33] R. L. Andrews, A. M. Heyns, P. M. Woodward, *Dalt. Trans.* **2015**, *44*, 10700.

[34] J. Hlinka, J. Petzelt, S. Kamba, D. Noujni, T. Ostapchuk, *Phase Transitions* **2006**, *79*, 41.

[35] A. Dias, G. Subodh, M. T. Sebastian, R. L. Moreira, *J. Raman Spectrosc.* **2009**, *41*, 702.

[36] B.-K. Kim, H. Hamaguchi, I.-T. Kim, K. S. Hong, *J. Am. Ceram. Soc.* **1995**, *78*, 3117.

[37] J. E. Rodrigues, D. M. Bezerra, A. C. Hernandes, *Ceram. Int.* **2017**, *43*, 14015.

[38] A. P. Ayala, I. Guedes, E. N. Silva, M. S. Augsburger, M. Del, C. Viola, J. C. Pedregosa, *J. Appl. Phys.* **2007**, *101*, 123511.

[39] N. S. N. Nath, *Proc. Indian Acad. Sci. - Sect. A* **1934**, *1*, 250.

[40] J. E. Rodrigues, D. M. Bezerra, R. C. Costa, P. S. Pizani, A. C. Hernandes, *J. Raman Spectrosc.* **2017**, *48*, 1243.

[41] C.-H. Wang, X.-P. Jing, L. Wang, J. Lu, *J. Am. Ceram. Soc.* **2009**, *92*, 1547.

[42] K.-R. Zhu, M.-S. Zhang, Q. Chen, Z. Yin, *Phys. Lett. A* **2005**, *340*, 220.

[43] L. Bergman, D. Alexson, P. Murphy, R. Nemanich, M. Dutta, M. Stroscio, C. Balkas, H. Shin, R. Davis, *Phys. Rev. B* **1999**, *59*, 12977.

[44] G. Gouadec, P. Colomban, *Prog. Cryst. Growth Charact. Mater.* **2007**, *53*, 1.

[45] S. Balaji, Y. Djaoued, J. Robichaud, *J. Raman Spectrosc.* **2006**, *37*, 1416.

[46] J. E. Spanier, R. D. Robinson, F. Zhang, S.-W. Chan, I. P. Herman, *Phys. Rev. B* **2001**, *64*, 245407.

How to cite this article: Rodrigues JE, Bezerra DM, Hernandes AC. Calculation of the optical phonons in ordered Ba_2MgWO_6 perovskite using short-range force field model. *J Raman Spectrosc.* 2018;49:1822–1829. https://doi.org/10.1002/jrs.5460